Lamellar Formation and Relaxation in Simple Sheared Poly(ethylene terephthalate) by Small-Angle X-ray Scattering

Zhi-Gang Wang,*,† Zhi-Yong Xia,‡ Zhen-Qiang Yu,§ Er-Qiang Chen,§ Hung-Jue Sue,‡ Charles C. Han,† and Benjamin S. Hsiao*,⊥

CAS Key Laboratory of Engineering Plastics, Joint Laboratory of Polymer Science and Materials, Institute of Chemistry, Chinese Academy of Sciences, Beijing 100080, China; Department of Mechanical Engineering, Texas A&M University, College Station, Texas 77843; Department of Polymer Science and Engineering, College of Chemistry and Molecular Engineering, Peking University, Beijing 100871, China; and Department of Chemistry, Stony Brook University, Stony Brook, New York 11794

Received September 4, 2005; Revised Manuscript Received February 2, 2006

ABSTRACT: Semicrystalline poly(ethylene terephthalate) (PET) was oriented with an equal channel angular extrusion (ECAE) process at room temperature, which applied simple shear deformation and generated unique asymmetric lamellar texture. In-situ small-angle X-ray scattering (SAXS) measurements were utilized to study the changes of lamellar structure during heating in samples with and without experiencing the simple shear deformation. The total scattered intensity, fractions of isotropic and anisotropic scattered intensities, orientation factors, and long periods along different shear directions were determined from 2-dimensional SAXS patterns. Orientation-stable α-lamellae with their normal perpendicular to the shear plane exhibited a larger long period after shear and a rapid decrease in long period upon heating, while less orientation-stable *β*-lamellae with their normal perpendicular to the flow direction exhibited a smaller long period after shear but only a slight decrease in long period upon heating. The thermally induced lamellar misorientaton could be attributed to the processes of lamellar relaxation and recrystallization of the amorphous phase. The possible molecular mechanisms for lamellar formation during simple shear are also discussed.

Introduction

The improvement of physical and mechanical properties in semicrystalline polymers, such as high modulus, high fracture toughness, good weatherability, and enhanced solvent resistance, can be achieved through the control of crystal morphology and orientation.[1−3] Recently, several studies have been carried out to demonstrate the varying pathways that can manipulate the morphology and orientation of semicrystalline polymers in the solid state.[1−4] In these studies, the use of an equal channel angular extrusion (ECAE) process (Figure 1) to control the morphology and crystal orientation of poly(ethylene terephthalate) (PET)[4] was of particular interest to us. This is because due to the unique nature of ECAE, a high level of simple shear deformation can be achieved in the solid material, generating an asymmetric arrangement of lamellar orientation. Compared with other solid-state polymer processing methods, such as drawing, hydrostatic extrusion, and rolling, the ECAE technique offers several advantages.[5−7] The advantages include the application of molecular orientation in bulk polymers without changing the geometry of the specimen; thus, different modes of molecular orientation in the extrudate can be obtained by changing the extrudate orientation through subsequent ECAE passes.

In this study, we have focused on one specific region of the ECAE process during deformation of PET: region II in Figure 1 (also Figure 1b in ref 4), where the material passes through the transitional line and experiences a high level of simple shear.

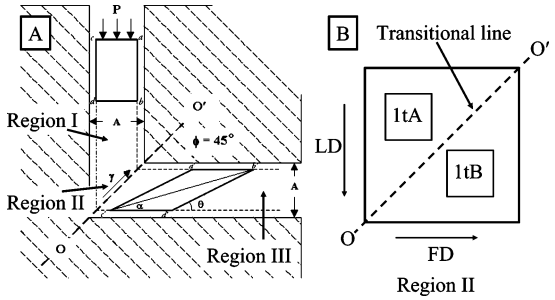

Figure 1. (A) Schematic of ECAE die showing the deformation of the billet. (B) Schematic of sample locations in region II of ECAE process. LD is loading direction, FD is flow direction, and dashed line is transitional line, where the sample experiences simple shear through ECAE process.

It is thought that the lamellar orientation can relax upon annealing; however, the degree of relaxation also depends on the initial lamellar orientation. To understand of this critical element of ECAE, a study of thermal stability and relaxation of the oriented lamellae obtained at this region during heating was carried out using the in-situ time-resolved synchrotron small-angle X-ray scattering (SAXS) technique. The SAXS measurement yielded real-time information about the morphological changes including the scattered intensity, lamellar long period, misorientation, relaxation, and orientation parameter during annealing. For comparison purposes, the samples obtained around the shear plane zone, i.e., above and below the transitional line in region II, respectively, have been investigated in this study.

Experimental Section

Sample Preparation by ECAE. PET (ENSITEP) sheets with a nominal thickness of 9.525 mm were obtained from Insinger Inc. The equal channel angular extrusion (ECAE) process[4,5] was used

† Chinese Academy of Sciences.
‡ Texas A&M University.
§ Peking University.
⊥ Stony Brook University.

* To whom correspondence should be addressed: Tel 011-86-10-62558172, Fax 011-86-10-62558172; E-mail: zgwang@iccas.ac.cn (Wang); Tel 01-631-632-7793, Fax 01-631-632-6518; E-mail: bhsiao@notes.cc.sunysb.edu (Hsiao).

10.1021/ma051928k CCC: $33.50
Published on Web 03/22/2006

to prepare the samples on the basis of the following procedures. The sheets were first cut into square specimens with dimensions of 152.40 mm × 152.40 mm × 9.525 mm to fit into the die for ECAE processing. The extrusion was performed at room temperature with an extrusion rate of 0.51 mm/s. The extrusion process was divided into three regions (Figure 1): region I, material was compressed but before passing through the right angle of the die; region II, material was in right angle area of the die; and region III, material was in the extruded region. The deformed specimens at the specific region II of ECAE were chosen for this study. Samples with dimensions of 1 mm × 1 mm × 0.2 mm were cut respectively from locations above (1tA) and beneath (1tB) the shear plane (transitional line OO′) on a partially extruded PET block. These samples were then polished slightly, marked with respect to the flow direction (FD), and oriented in the small-angle X-ray scattering (SAXS) setup with the incident X-ray beam aligned perpendicularly to the sample plane. Using this geometry, the two-dimensional (2D) SAXS pattern could directly probe the anisotropy distribution of the lamellar stacks in the sample plane. An additional sample of 1 mm × 1 mm × 0.2 mm was also cut at the location after the transitional line, having the normal of the sample plane parallel to the shear plane. This sample was prepared to verify the axial symmetrical distribution of lamellar stacks. For this sample, the incident X-ray beam would be along the direction within the shear plane. A single 2D SAXS pattern was recorded for this sample.

Small-Angle X-ray Scattering. Time-resolved small-angle X-ray scattering (SAXS) measurements using a MAR CCD X-ray detector were performed at the Advanced Polymers Beamline (X27C) in the National Synchrotron Light Source, Brookhaven National Laboratory. The detailed experimental setup for SAXS and the high-temperature hot stage have been described in previous publications.[8,9] The sample temperatures during heating were carefully calibrated by several standard crystal samples including isotactic polypropylene (iPP) and polyethylene (PE). The uncertainty of temperature in this study was 1 °C.

The SAXS experimental procedures were as follows. The sample was heated from 60 to 165 °C at a rate of 5 °C/min. Time-resolved SAXS measurements were performed with a data acquisition time of 60 s per image. The sample-to-detector distance was 1730 mm. The X-ray wavelength was 1.366 Å. All SAXS images were corrected for the main beam intensity fluctuations and sample absorption. The angular position of the SAXS profile was calibrated by the silver behenate standard.

Wide-Angle X-ray Diffraction. To compare the orientation of lamellar stacks with that of PET crystals, 2D wide-angle X-ray diffraction (WAXD) patterns of samples 1tA and 1tB were also acquired using a Bruker D8 Discover diffractometer equipped with GADDS as the 2D detector. Samples were mounted on the sample stage, and the point-focused X-ray beam was aligned perpendicular to the sample plane. The 2D WAXD patterns were recorded in a transmission mode at room temperature. The calibration was conducted using silicon powder and silver behenate as standards.

Results

Time-Resolved SAXS Study during Heating. Parts a and b of Figure 2 show two selected series of 2D SAXS patterns of samples 1tA and 1tB during heating, respectively. These SAXS patterns have been corrected for background scattering (air). The ECAE-processed PET samples above and beneath the transitional line (Figure 1) exhibited totally different scattering patterns. The SAXS patterns above the transition line (sample 1tA) were almost isotropic (Figure 2a), while those below the transition line (sample 1tB) were anisotropic with discrete scattering features (Figure 2b). All patterns exhibited the scattering maximum, indicating the existence of a lamellar structure in the semicrystalline PET. This is consistent with our previous result on the lamellar stacks in these PET samples observed by transition electron microscopy and atomic force microscopy measurements.[4,10−12]

In sample 1tA, the majority of the lamellae were isotropically distributed, suggesting that the lamellae within the spherulites did not experience the shear deformation above the shear plane (Figure 2c). In contrast, in sample 1tB, a unique four-spot SAXS pattern, having one pair of nearly symmetric spots aligned along the 128° (α) azimuthal angular axis and another pair of antisymmetric peaks aligned along the 81° (*β*) azimuthal angular axis (Figure 2c), was seen. These two axes (α and *β*) are consistent with the angular assignment in the previous ECAE study;[4] i.e., the 81° direction almost coincides with the normal of the flow direction, while the 128° axis is parallel to the normal of the shear plane. The phrase "antisymmetric" was used to describe the asymmetric nature of the scattering maxima along the 81° axis. The SAXS patterns in sample 1tB indicate the presence of two dominant populations (we term them α- and *β*-lamellae) of lamellar stacks, which are very different from the randomly distributed lamellar stacks in sample 1tA. The principal normals of α- and *β*-lamellae are basically perpendicular to the shear plane and the flow direction, respectively. This can be explained by the following argument. The average modulus of the crystalline PET lamellar stack (which can be viewed as an integrated entity) is significantly larger than that of the surrounding amorphous matrix. Thus, when the PET sample passes through the transitional line during the ECAE process, randomly distributed lamellar stacks have a tendency to reorient themselves along two principal flow directions (i.e., the flow plane and the shear plane). The α-lamellae (symmetric spots along the 128° axis) are formed when the lamellar stacks are aligned along the shear plane (or the normals are perpendicular to the shear plane). It appears that the α-lamellae have a relatively narrow azimuthal distribution. The *β*-lamellae (asymmetric spots along the 81° axis) are formed when the lamellar stacks are aligned along the flow plane (or the normals are perpendicular to the flow plane). It was seen that the scattered intensity from the α-lamellae is higher than that from the *β*-lamellae.

In Figure 2, it is seen that the scattered intensity, the position of the scattering maximum, and scattering orientation all change with temperature for both 1tA and 1tB samples during heating. The corresponding morphological parameters, such as total scattered intensity, fractions of isotropic and anisotropic components, long periods of the lamellar stacks, azimuthal angles at the scattering peaks, and orientation factor, during heating can be extracted from the SAXS patterns, which will be discussed below.

Fractions of Isotropic and Anisotropic Components. Using a 2D SAXS deconvolution procedure developed in our group,[13] the total scattered intensity, after correction of background and air scattering (Figure 3a-A), was separated into two fractions: the anisotropic contribution $A_{an}(q)$ (from oriented structures) (Figure 3a-B) and the isotropic contribution $A_{iso}(q)$ (from unoriented structures) (Figure 3a-C). The isotropic fraction $A_{iso}(q)$ was obtained using the "halo" method, which is briefly described as follows. Starting from the center of the scattering origin, an azimuthal scan was drawn along the angular axes (2θ). At each angular pixel position, a minimum scattered intensity value was obtained from the azimuthal scan, yielding an intensity envelope of the isotropic fraction moving along the angular axis. The deconvolution of the anisotropic fraction $A_{an}(q)$ is based on eq 1

$$A = A_{iso}(q) + A_{an}(q) \quad (1)$$

where A is the total scattered intensity and $q = 4\pi/\lambda \sin\theta$ is

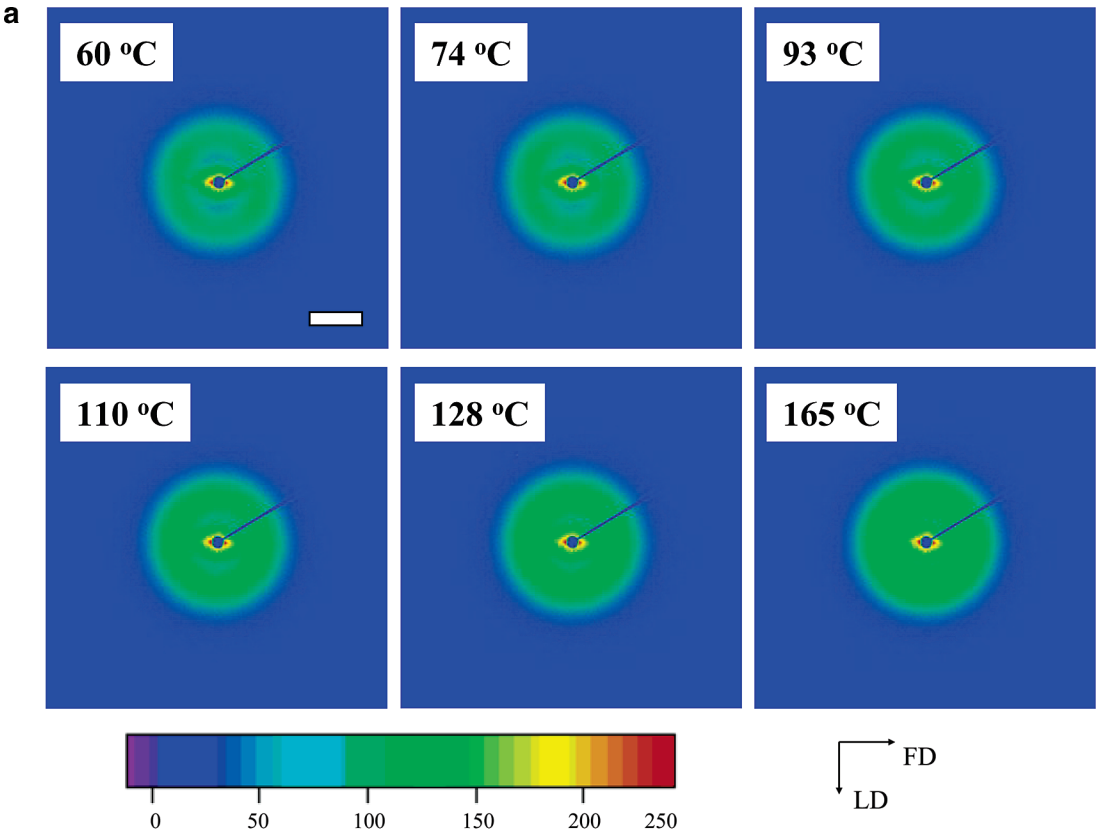
a
60 °C
74 °C
93 °C
110 °C
128 °C
165 °C
0
50
100
150
200
250
FD
LD
b
62 °C
84 °C
108 °C
132 °C
144 °C
161 °C
FD
LD

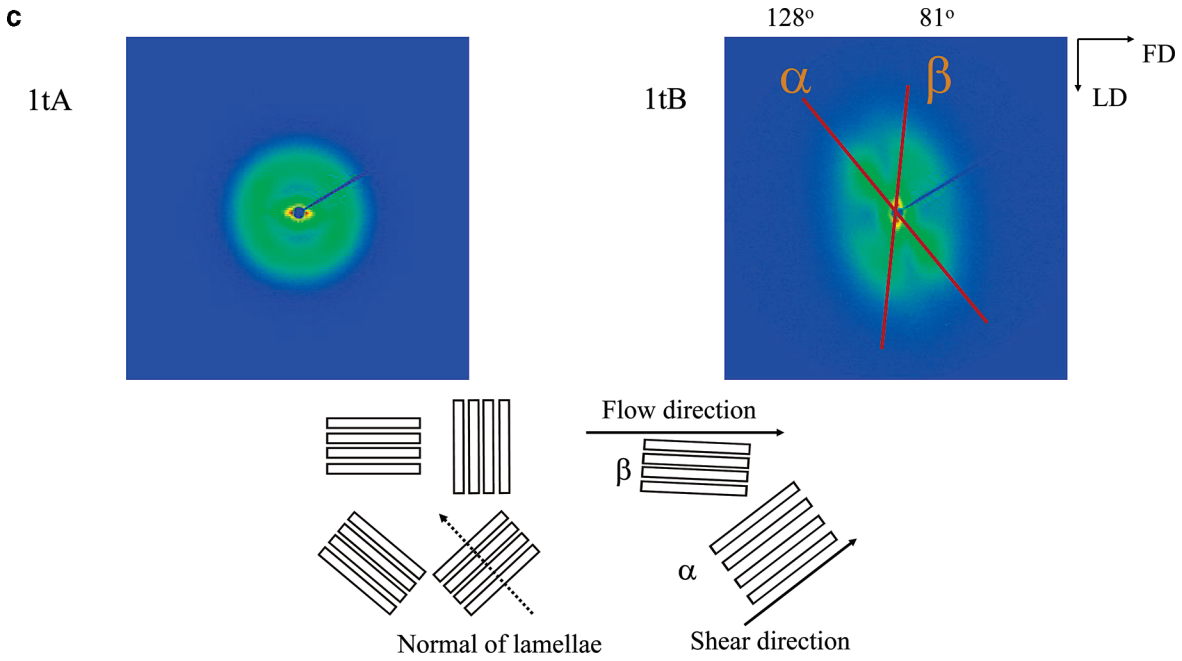

Figure 2. Selected 2-dimensional SAXS patterns during heating for sample 1tA (a) and sample 1tB (b) and schematic of orientation of the lamellar stacks in samples 1tA and 1tB (c). The white bar in (a) represents a q value of 0.06 Å^{-1}.

the magnitude of the scattering vector with 2θ being the scattering angle.

Figure 3b,c shows the results from the above analysis. In sample 1tA, the total scattered intensity began to increase at temperature above 80 °C (Figure 3b), which is close to the glass transition temperature (T_g) of PET. This behavior can be explained by the following two events: (1) the development of unoriented structures from the recrystallization process and (2) the increase in the density contrast between the crystal and amorphous phases. Since the sample 1tA (cut above the transitional line) have only experienced a low level of deformation, both melting and subsequent recrystallization processes are expected to occur above T_g (recrystallization of PET above T_g has been demonstrated by us previously using time-resolved wide-angle X-ray diffraction (WAXD) technique[14]), which would increase the total scattered intensity. On the other hand, the enhanced density contrast between the crystal and amorphous phases at high temperatures is due to the different thermal expansion coefficients of the two phases.

It was seen that the scattered intensity of the anisotropic fraction in sample 1tA remained about constant during heating (Figure 3b). The anisotropic fraction in sample 1tA was mainly from the central portion (eyelike) of the SAXS pattern, in which this anisotropic scattering feature persisted even when the sample was heated to above 300 °C. Because the equilibrium melting temperature of PET crystals is about 280 °C, the central eyelike scattering feature cannot be related to PET crystal lamellar stacks. We believe that the chosen PET sample might contain certain types of aggregates, formed by the presence of foreign additives, having sizes detectable by SAXS and surviving above 300 °C. As the central scattering was constant above the melting point and it was positioned at a much lower scattering angle than the scattering peak from the PET lamellar stacks, its existence overall did not affect the results and discussion related to the PET lamellar stacks in this study.

During heating, the changes of scattered intensities in sample 1tB were different from those in sample 1tA. For instance, the total scattered intensity of sample 1tB began to increase above 120 °C, and the corresponding increase (mainly due to the intensity rise of the isotropic fraction) was smaller than that of sample 1tA (Figure 3b). However, the scattered intensity of the isotropic fraction began to increase above 80 °C, which was similar to that in sample 1tA. In addition, the scattered intensity of the anisotropic fraction was found to first decrease at 80 °C and then increase above 120 °C. The opposite changes of the isotropic and anisotropic fractions below 120 °C resulted in a constant value of total scattered intensity at temperatures below 120 °C in sample 1tB. This behavior can be explained as follows. When temperature is above 80 °C (i.e., T_g of PET), the chain segments in the amorphous region become mobile, resulting in relaxation and melting of the initial lamellae (mostly oriented) and reduction of the scattered intensity of the anisotropic fraction. The subsequent recrystallization can generate both oriented and unoriented crystallites, which would increase both scattered intensities of isotropic and anisotropic fractions. The relative changes of the isotropic and anisotropic fractions are more significant in sample 1tB than sample 1tA.

Time-Resolved SAXS Profiles and Evolution of Lamellar Long Periods. Because of the anisotropic nature of the 2D SAXS patterns, linear intensity profiles along selected axes are illustrated in Figure 4. Figure 4a shows the scattered intensity profiles of sample 1tA (with a low degree of anisotropy) along the equatorial and meridional axes at different temperatures. The scattering maximum was clearly observed, and the peak position remained about constant during heating. The intensity profile along the equatorial direction consisted of a much stronger low-angle scattering upturn than that along the meridional direction. The low-angle scattering upturn (close to the beam stop) indicates the existence of morphological feature at a large scale (i.e., thousands of angstroms), which may be partially related to the aggregates formed from foreign additives or cavities having sizes larger than the lamellar long period but still within the detection range of the SAXS setup. In addition, the upturn may also be related to the interference among the lamellar stacks, which has been observed in similar semicrystalline systems before.[15] As stated earlier, the low-angle scattering upturn did not affect the results and discussion related to the PET lamellar stacks hereafter.

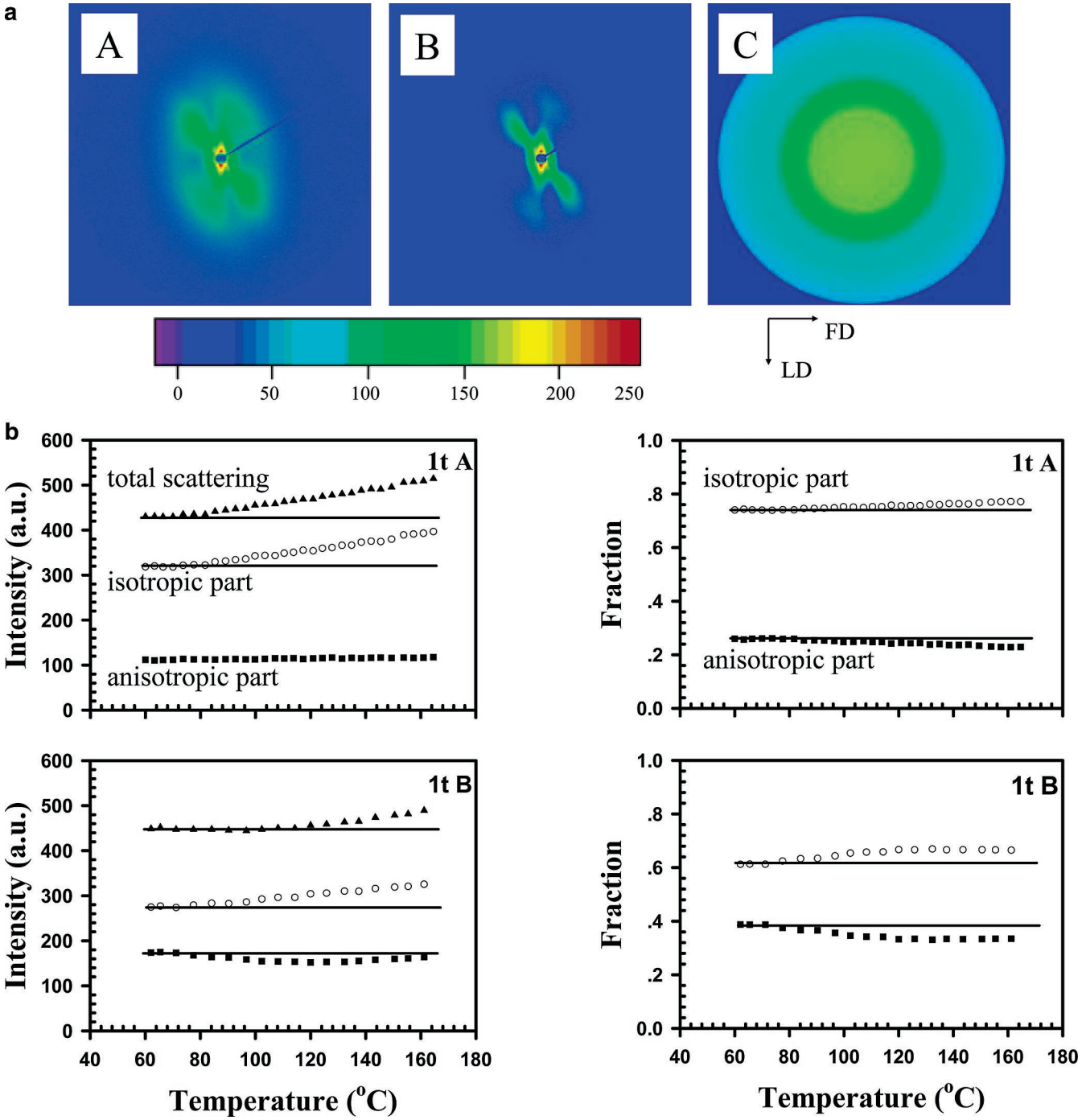

Figure 3. (a) Image analysis procedure to separate the isotropic and anisotropic fractions, using SAXS pattern of sample 1tB at 62 °C as the example: (A) total SAXS pattern, (B) anisotropic part, (C) isotropic part; (b) changes of scattered intensity of the total, anisotropic and isotropic SAXS during heating for samples 1tA and 1tB; (c) changes of anisotropic and isotropic fractions during heating for samples 1tA and 1tB. The solid lines in (b) and (c) are guides to the eye.

Figure 4b shows the intensity profiles of sample 1tB around the 128° and 81° axes. We note that during heating the scattering maximum actually deviated from the 128° and 81° axes, where the profiles in Figure 4b were obtained at the azimuthal angular axes showing the strongest scattered intensities. It was seen that in the profiles around the 128° axis the position of the scattering peak shifted to a larger q value during heating, indicating the decrease of the lamellar long period with temperature. From the linear intensity profile, the most probable long period (L_B) was estimated using Bragg's law to analyze the position of scattering maximum in the Lorentz-corrected intensity profile, and the scattering invariant (Q) was calculated using eq 2.

$$Q = \int_{q_1}^{q_2} I(q) q^2 \, dq \qquad (2)$$

In eq 2, the values of q_1 (~0.005 Å^{-1}) and q_2 (~0.20 Å^{-1}) represent the limitations of the experimental setup. The values of Q can be conveniently used to compare the scattering power during time-resolved experiments because all scattering profiles were corrected for the sample thickness, absorption, beam fluctuations, and air scattering.

Results of L_B and Q for both samples 1tA and 1tB at varying temperatures are shown in Figure 5. For sample 1tA, the values

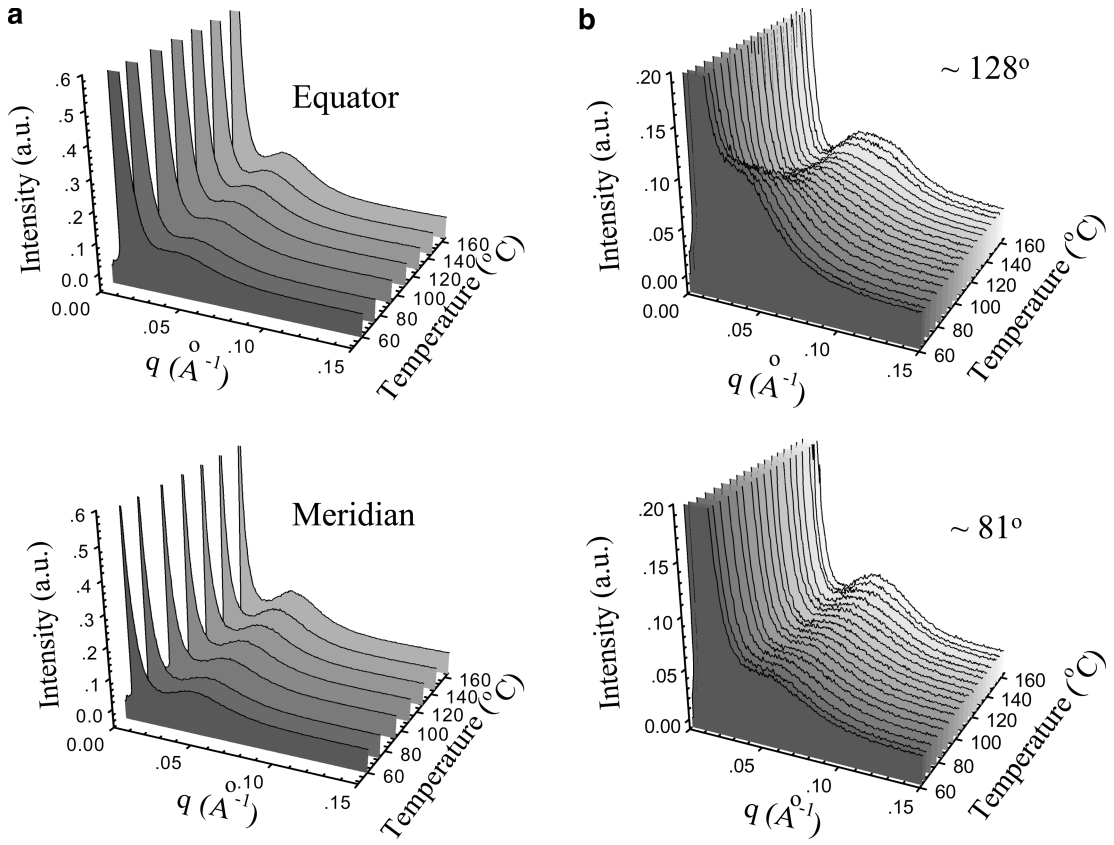

Figure 4. (a) SAXS 1-D intensity profiles along equator and meridian for sample 1tA. (b) SAXS 1-D intensity profiles along 128° and 81° directions for sample 1tB.

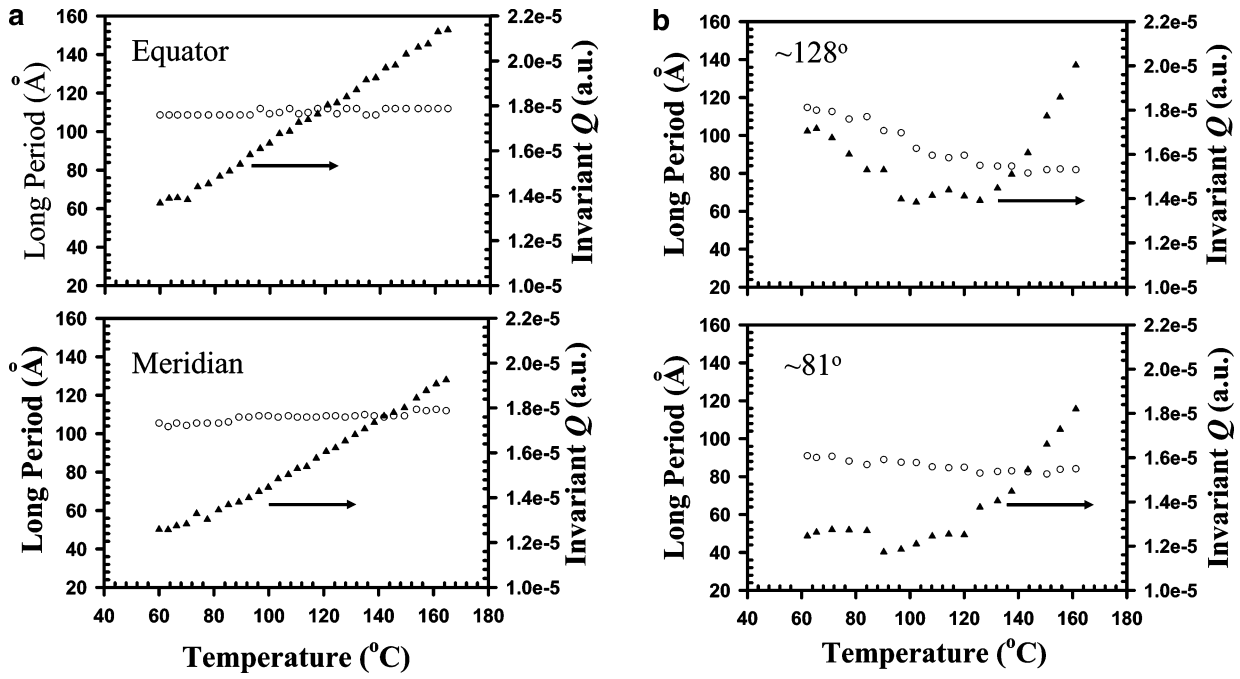

Figure 5. (a) Changes of long period (○, L_B) and 1-D scattering invariant (▲, Q) along equator and meridian for sample 1tA. (b) Changes of long period and 1-D scattering invariant along 128° and 81° directions for sample 1tB.

of L_B along the equator and the meridian were very similar (104−108 Å), and both increased very slightly during heating (Figure 5a). The scattering invariant Q also exhibited a similar trend in both directions. That is, above the T_g, the scattering invariant Q increased rapidly, consistent with the change of the total scattered intensity in Figure 3b. For sample 1tB, the process of heating showed a more complicated effect on the changes of lamellar long period and scattering invariant. For example, in Figure 5b, the initial long periods exhibited the following values: ∼114 Å for the α-lamellae and ∼90 Å for the β-lamellae (we note that the long period of the isotropic lamellae in sample 1tA was 104−108 Å). It appeared that after passing through the transitional line some lamellae experienced expansion and formed α-lamellae, while some experienced contraction and formed β-lamellae. In ECAE, the lamellar thickening mechanism is thought to be difficult to occur because the

experimental temperature (room temperature) is way below the T_g of PET. Furthermore, the selection of thicker lamellar stacks to aggregate and form α-lamellae during simple shear is very unlikely. Thus, the apparent long period expansion and contraction resulting in two populations of lamellar stacks must be due to the variations of the amorphous layers within the lamellar stacks. As to be discussed later, the two populations of lamellae (α and β) were formed mainly through the combination of (1) lamellar deformation (the major mechanism) through interlamellar extension (by sliding) or compression of the amorphous layers in the lamellar stacks and (2) the recrystallization process producing new crystalline lamellae (the minor mechanism). In Figure 5b, the long period of the α-lamellae showed a dramatic decrease from 114 to 86 Å when temperature was increased from 60 to 120 °C; above 120 °C, the long period was about constant (86−84 Å). In contrast, the long period of the β-lamellae showed only a slight decrease from 90 to 86 Å from 60 to 120 °C and remained about constant at 84 Å above 120 °C. The large decrease of the α-lamellae with temperature could be related to the significant chain relaxation in the amorphous layers.

It was interesting to note that around the 128° axis the scattering invariant Q showed a decrease from 60 to 100 °C, remained about constant from 100 to 128 °C, and increased abruptly above 128 °C. The corresponding Q change around the 81° axis exhibited a similar trend but with slightly different transition regions and scattering strength. For example, in the Q value around the 81° axis, a slight decrease was seen below 90 °C, followed immediately by a small increase from 90 to 120 °C and then a significant increase above 120 °C. The changes of the Q values in Figure 5b were different from the changes of the total scattered intensity during heating in sample 1tB (Figure 3b), which can be explained by considering both lamellar misorientation at low temperatures and recrystallization of the amorphous phase at high temperatures. It is thought that thermal relaxation of the amorphous layer between the oriented lamellae can take place at low temperatures (e.g., below 100 °C) and causes aligned lamellae to randomize. The misorientation of lamellar stacks can decrease the invariant of the 1D SAXS profile, but it would not change the total scattered intensity. As the α-lamellae showed a higher degree of misorientation, it would result in larger decreases of the lamellar long period and the scattering invariant than those in the β-lamellae. On the other hand, recrystallization can take place at high temperatures, and it would increase both total scattered intensity and 1D scattering invariant.

Relaxation of Lamellar Orientation upon Heating. To evaluate the relaxation behavior of oriented lamellae produced by ECAE, azimuthal intensity profiles at the scattering maximum from the 2D SAXS patterns were taken at different temperatures. Figure 6 illustrates the procedure of such an analysis, in which the solid line represents the flow direction (the azimuthal angle was taken counterclockwise). Based on this procedure, selected azimuthal intensity profiles for sample 1tB at different temperatures are displayed in Figure 7a, and the corresponding changes of the azimuthal angle for the scattering maximum are shown in Figure 7b. It was seen that at low temperatures (less than 120 °C) the maximum scattered intensities of peaks 2 and 4 were much higher than those of peaks 1 and 3 (Figure 7a), indicating the dominance of the α-lamellae. In addition, peaks 2 and 4 exhibited much narrower peak widths than peaks 1 and 3, suggesting a narrower distribution of the lamellar orientation for α-lamellae than β-lamellae (peaks 1 and 3 were asymmetric). During heating, the maximum intensities

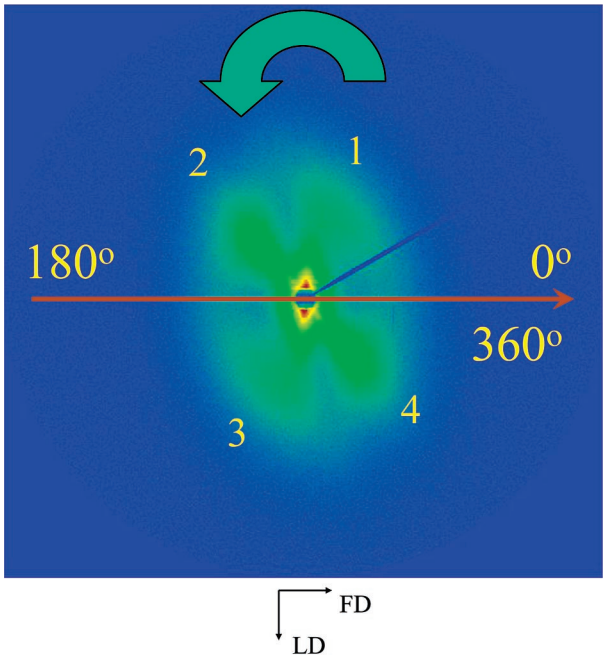

Figure 6. Assignment of the azimuthal angle in 2D SAXS pattern using sample 1tB at 62 °C as an example.

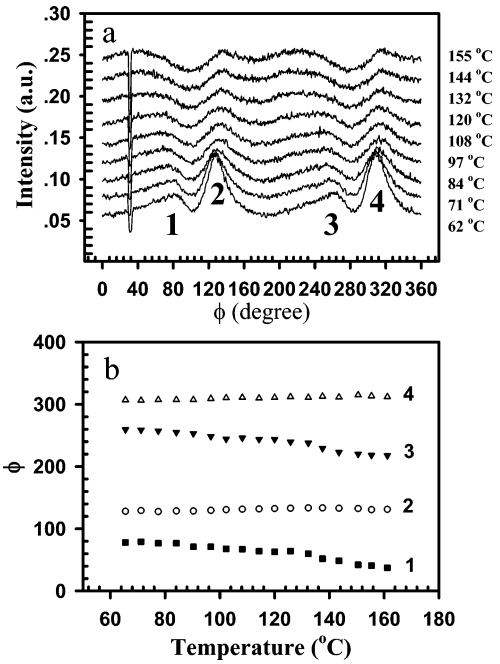

Figure 7. (a) Selected azimuthal intensity profiles and (b) changes of azimuthal angles of four SAXS spots for sample 1tB during heating.

of these four peaks became similar, especially at temperatures higher than 120 °C. However, the α-lamellae consistently showed a narrower peak width than β-lamellae. In Figure 7b, the azimuthal angles of peaks 2 and 4 were relatively stable with temperature, but the angles of peaks 1 and 3 were found to decrease with temperature, especially above 120 °C. These results indicate that the α-lamellae are relatively thermally stable, while the β-lamellae tend to tilt away of the flow direction. As a result, the difference of the azimuthal angles for the α- and β-lamellae became greater with temperature.

The approach outlined by Keates et al.[16] was used to evaluate the orientation parameter from the SAXS patterns in this study. In the approach, the orientation factor of an assembly of

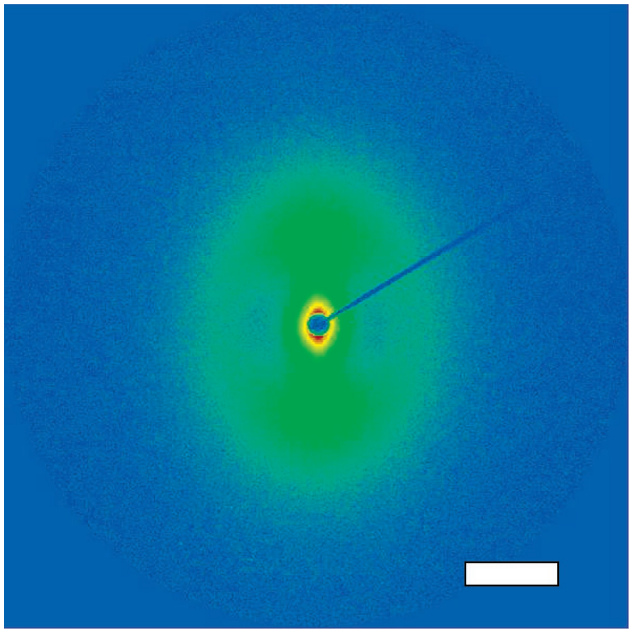

Figure 8. SAXS pattern of the sample cut after the transitional line with the normal of the sample plane is parallel to the shear plane. The white bar represents q value of 0.06 Å^{-1}.

lamellae, $\langle \cos^2 \phi \rangle_{Av}$, was calculated using the following equation:

$$\langle \cos^2 \phi \rangle_{Av} = \int_0^{\pi/2} I(\phi) \cos^2 \phi \sin \phi \, d\phi / \int_0^{\pi/2} I(\phi) \sin \phi \, d\phi \quad (3)$$

where $I(\phi)$ represents the scattered intensity at the azimuthal angle ϕ. The orientation parameter $\langle \cos^2 \phi \rangle_{Av}$ has a value of unity when all the lamellae are oriented with their normals parallel to the reference direction and a value of zero when their normals are perpendicular to the reference direction (here the reference direction is the normal of the shear plane for the α-lamellae as shown in Figure 2c). The Hermans orientation function,[17] $\langle P_2(\cos \phi) \rangle$, was used to describe the degree of orientation:

$$\langle P_2(\cos \phi) \rangle = (3\langle \cos^2 \phi \rangle - 1)/2 \quad (4)$$

where $\langle P_2(\cos \theta) \rangle$ has a value of unity when all the lamellae are oriented with their normals parallel to the reference direction, a value of −0.5 when all the lamellae are oriented with their normals perpendicular to the reference direction and a value of zero when there is no preferred orientation of the lamellae. We note that the proper application of the Hermans orientation function for the above SAXS analysis requires that the distribution of the lamellar normals must have an axial symmetry. For the α-lamellae, this axis is the normal to the shear plane. To verify this scenario, a SAXS pattern was recorded using a sample (1 mm × 1 mm × 0.2 mm) cross sectioned after the transitional line with the incident X-ray beam orthogonal to the shear plane and the lamellar normal. This pattern is illustrated in Figure 8, where the scattering feature indicates that the normals of the α-lamellae indeed had an axial symmetry. Therefore, the use of Hermans orientation function is justified to estimate the orientation parameter for the lamellar stacks.

The azimuthal intensity peak around the 128° axis (corresponding to peak 2) was used to calculate the Hermans orientation function $\langle P_2 \rangle$ (eq 4). This function represents the orientation distribution of the α-lamellae with their normals 128° away of the flow direction (orientation of the β−lamellae with their normals 81° away of the flow direction was not calculated because peaks 1 and 3 did not exhibit an axial symmetry). Results of $\langle P_2 \rangle$ at different temperatures are shown in Figure 9. It was seen that the initial degree of orientation for the α-lamellae having their normals perpendicular to the shear plane was high (∼0.93), which began to decrease linearly above 85 °C and reached a value of 0.8 at 160 °C. The onset temperature where misorientation of the α-lamellae occurred coincided with the T_g of PET. Furthermore, the recrystallization process at high temperatures produced a new population of lamellae with less degree of orientation, which also decreased the total degree of orientation (Figure 9).

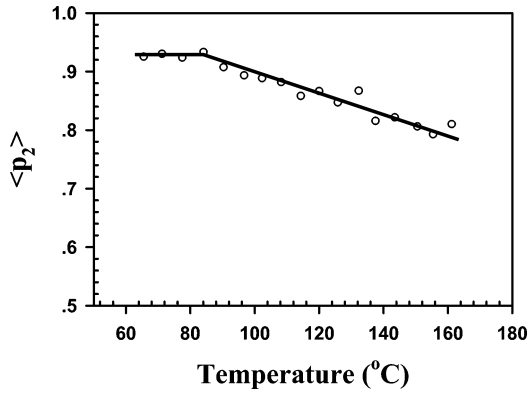

Figure 9. Change of the degree of orientation of the α-lamellae with their normals perpendicular to the shear plane for sample 1tB during heating.

Verification Crystal Orientation by WAXD. The technique of wide-angle X-ray diffraction (WAXD) has been routinely used to estimate the crystal orientation of polymers[17] such as PET.[18] However, the crystal orientation determined by WAXD and the lamellae orientation determined by SAXS may not be the same. It is conceivable that the crystallographic axis can become tilted and even melt away in lamellae at higher temperatures, while the lamellar structure can remain intact, as in some cases of block copolymers. On the other hand, it is also possible that the lamellar structure can be distorted first while the crystal structure can remain at high temperature, as in some case of polymer blends.

Although the goal of this work is to study the lamellar structure changes during the ECAE process and upon subsequent heating, we have also carried out static WAXD measurements on samples deformed above and below the transitional line (Figure 10). The corresponding azimuthal intensity scans taken at the diffraction peak of (−110) for the two samples are shown in Figure 11. Results confirmed that PET crystals in the sample 1tA were basically isotropic, but PET crystals in the sample 1tB were partially oriented. The Hermans orientation function determined by the (−110) reflection in the WAXD image in sample 1tB was consistent with that determined by the peak 2 (i.e., the α-lamellae) in the SAXS pattern (Figure 9). This indicates that the orientation of the normal to the (−110) plane is consistent with the normals of the α-lamellae. The SAXS image of the sheared sample after ECAE clearly exhibited the existence of two populations of lamellae with different orientations; however, the corresponding WAXD image was dominated by crystal structure from the α-lamellae. This indicates that the crystal structure of the β-lamellae was poor or/and the amount was low.

Discussion

A number of studies have been carried out to investigate the relationships between the morphology and mechanical properties

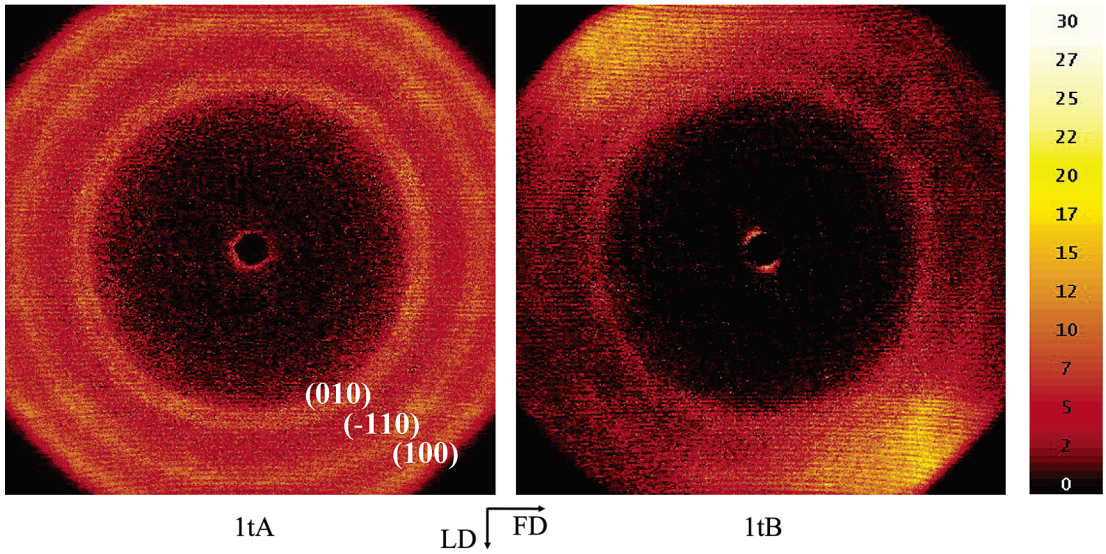

Figure 10. WAXD patterns of samples 1tA and 1tB. The 2θ range for each pattern is from 0 to 26°.

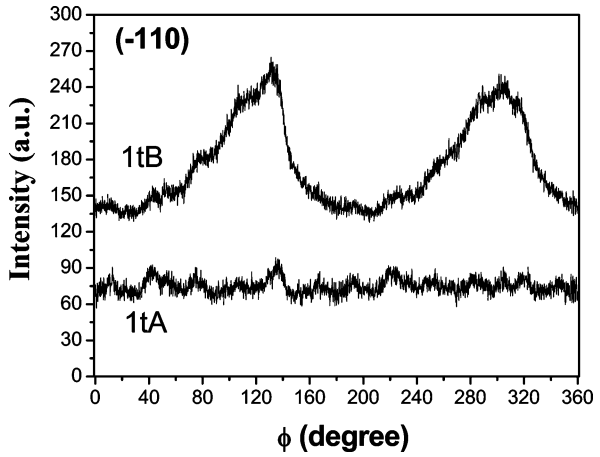

Figure 11. Azimuthal intensity profiles for samples 1tA and 1tB taken at the (−110) reflection position from the WAXD patterns.

under deformation for semicrystalline polymers, such as high-density polyethylene (HDPE), nylon-6, and PET.[19−21] In these studies, it was generally concluded that the crystalline phase is deformed mainly by the crystallographic shear mechanism. In a recent study of the mechanically rolled PET,[22] it was reported that crystallographic shear did not necessarily require the dislocation motion owing to the relatively weak bonds between the neighboring polymer segments in the crystals.

Bellare et al. performed a comprehensive study on the interplay between the crystallographic shear and the development of deformed textures in PET under planar strain conditions.[23] They pointed out that during deformation the initial spherulitic morphology was rendered into stacks of fragmented crystal lamellae with their normals oriented toward the flow direction by interlamellar sliding in the amorphous layers. Only at the later deformation stage, the crystallographic shear became dominant. The experimental results from Bellare et al. have also been described by simulation.[24] The predominant crystallographic shear mechanism was also found in the rolled PET samples. During rolling experiments of PET at room temperature, continuous strain-induced amorphization of the crystalline phases was observed.[22] One possible explanation is that the sheared lamellae break apart into sets of crystalline blocks, containing severe lattice defects.[25] This process has been referred as "mechanical melting". In a way, an intermediate phase is produced by uniaxial deformation, having ordering between those of crystalline and amorphous phases as suggested by Strobl et al.[26−30] It appears that at small strains interlamellar sliding in amorphous layers is the dominant deformation mechanism, while at large strains (above yielding), the strain-induced crystalline disintegration (mechanical melting) and subsequent recrystallization take place.

On the basis of the previous study of ECAE[4] and the SAXS results in this work (Figure 2), it is clear that two distinct populations of lamellae with different orientations are induced by the ECAE deformation: the α-lamellae with their normals perpendicular to shear plane and the β-lamellae with their normals perpendicular to the flow direction. Two observations were helpful to understand the deformation mechanism for the solid-state orientation of semicrystalline PET. One was that the population of the β-lamellae was relatively less than the α-lamellae, as shown by the weaker SAXS intensity of β-lamellae. Another was that the long period of the β-lamellae was narrower (90 Å) than that in the initial state (sample 1tA, 104−108 Å), while the long period of the α-lamellae was wider (114 Å). The first observation can be explained as follows. Upon passing through the shear plane (the OO′ in Figure 1), the initial spherulite morphology with randomly distributed lamellar orientation is destroyed. However, the lamellar structures are not affected in the same manner. The lamellae with the normal perpendicular to the principal deformation planes (i.e., the shear plane and the flow plane) will experience the least deformation, while the ones with the normal parallel to the principal deformation planes will experience the most deformation. The lamellae with intermediate orientation will experience deformation in between the two extremes. During lamellar deformation, interlamellar sliding, crystallographic shear, and shear-induced disintegration of crystalline lamellae can all take place, depending on the level of the local strain. As the shear motion is the principal deformation in the ECAE process, the majority of the lamellae would end up with normal perpendicular to the shear plane (i.e., the α-lamellae). The comparison of the different long periods between the deformed and undeformed samples indicates that the α-lamellae are primarily formed by interlamellar sliding in the amorphous layers, which increases the long periods, while the β-lamellae are primarily formed by shear compression, which would decrease the long period. However, it is conceivable that recrystallization would also occur during deformation,[31] generating new lamellae with long periods much smaller than that of undeformed sample (as they are produced at room

temperature). We envision that the strain-induced crystallization process may be a secondary mechanism compared to the primary interlamellar shearing mechanism. Results from this study clearly indicate that the catastrophic "destruction−reconstruction" mechanism is not suitable to describe the deformation mechanism in ECAE at room temperature.

The heating experiments probed the thermal stability of these two types of lamellae (α-lamellae and *β*-lamellae). In the α-lamellae, the large decrease of the long period above T_g can be attributed to the relaxation of the amorphous interlamellar chains, which is consistent with the hypothesis that these lamellae are formed mainly through the interlamellar sliding mechanism. SAXS results indicate that the α-lamellae became misorientated upon heating. This behavior is consistent with a WAXD study of PET fibers, which showed the decrease of the crystal orientation at the late stages of annealing.[32] It is anticipated that the lamellar misorientaton accompanies the crystal misorientaton. However, the exact relationship between these two structures with different scales needs further investigation. The less populated *β*-lamellae also exhibited a decrease in long period upon heating, which may be partially due to the recrystallization process, resulting in lamellar stacks with small long periods.

Conclusions

The simple shear through an equal channel angular extrusion (ECAE) process has been used to generate the oriented lamellar texture in semicrystalline PET at room temperature. Two populations of lamellae were observed in the sheared sample by SAXS: a larger population of α-lamellae with the normals perpendicular to the shear plane and a smaller population of the *β*-lamellae with the normals perpendicular to the flow direction. These two lamellar populations are formed through the combination of interlamellar sliding (the major mechanism) and shear-induced crystallization (the minor mechanism). Time-resolved SAXS experiments were employed to follow the changes of lamellar orientation, long period, and fractions of isotropic and anisotropic components in the sheared PET sample during heating. The α-lamellae exhibited a larger average long period with a more rapid decrease during heating, whereas the *β*-lamellae exhibited a smaller long period with less decrease. In addition, lamellar misorientation was observed at temperatures above T_g. These results can be attributed to the lamellar relaxation and recrystallization of the amorphous phase.

Acknowledgment. Z.-G. Wang acknowledges the financial support from "Hundreds Young Talents" Program of Chinese Academy of Sciences and the National Science Foundation of China with Grant NSFC 10590355. He also thanks Professor Jerold M. Schultz at University of Delaware and Dr. Liangbin Li at Unilever Research Center in The Netherlands for providing helpful suggestions and discussions. B. S. Hsiao thanks the financial support of this work by the National Science Foundation (DMR-0405432). The authors gratefully acknowledge Dr. Dufei Fang for supplying the X-ray image analysis software, POLAR.

References and Notes

(1) Thomas, L. S.; Cleereman, K. J. *SPE J.* **1972**, *28*, 61.
(2) Southern, J. H.; Porter, R. S. *J. Appl. Polym. Sci.* **1970**, *14*, 2305.
(3) Iwata, T.; Doi, Y. *Macromol. Chem. Phys.* **1999**, *200*, 2429.
(4) Xia, Z.-Y.; Sue, H.-J.; Rieker, T. P. *Macromolecules* **2000**, *33*, 8746.
(5) Xia, Z.-Y. Ph.D. Dissertation, Texas A&M University, College Station, 2001.
(6) Sue, H.-J.; Li, C. K. Y. *J. Mater. Sci., Lett.* **1998**, *17*, 853.
(7) Li, C. K. Y.; Xia, Z.-Y.; Sue, H.-J. *Polymer* **2000**, *41*, 6285.
(8) Sue, H.-J.; Dilan, H.; Li, C. K. Y. *Polym. Eng. Sci.* **1999**, *39*, 2505.
(9) Hsiao, B. S.; Chu, B.; Yeh, F. NSLS July Newsletter, 1997, 1; http://bnlx27c.nsls.bnl.gov.
(10) Song, H. H.; Wu, D. Q.; Chu, B.; Satkowski, M.; Ree, M.; Stein, R. S.; Phillips, J. C. *Macromolecules* **1990**, *23*, 2380.
(11) Wang, Z. G.; Hsiao, B. S.; Sauer, B. B.; Kampert, W. G. *Polymer* **1999**, *40*, 4615.
(12) Wang, Z. G.; Hsiao, B. S.; Fu, B. X.; Liu, L.; Yeh, F.; Sauer, B. B.; Chang, H.; Schultz, J. M. *Polymer* **2000**, *41*, 1791.
(13) Ran, S.; Zong, X.; Fang, D.; Hsiao, B.; Chu, B.; Ross, R. *J. Appl. Crystallogr.* **2000**, *33*, 1031.
(14) Ran, S.; Wang, Z. G.; Burger, C.; Chu, B.; Hsiao, B. S. *Macromolecules* **2002**, *35*, 10102.
(15) Vignaud, R.; Schultz, J. M. *Polymer* **1986**, *27*, 651.
(16) Keates, P.; Mitchell, G. R.; Peuvrel-Disdier, E.; Navard, P. *Polymer* **1993**, *34*, 1316.
(17) Alexander, L. E. *X-ray Diffraction Methods in Polymer Science*; Wiley: New York, 1969.
(18) Kawakami, D.; Ran, S.; Burger, C.; Fu, B.; Sics, I.; Hsiao, B. S.; *Macromolecules* **2003**, *36*, 9275.
(19) Bartczak, Z.; Argon, A. S.; Cohen, R. E. *Macromolecules* **1992**, *25*, 5036.
(20) Lin, L.; Argon, A. S. *Macromolecules* **1992**, *25*, 4011.
(21) Asano, T.; Balta Calleja, F. J.; Flores, A.; Tanigaki, M.; Mina, M. F.; Sawatari, C.; Itagaki, H.; Takahashi, H.; Hatta, I. *Polymer* **1999**, *40*, 6475.
(22) Raabe, D.; Chen, N.; Chen, L. *Polymer* **2004**, *45*, 8265.
(23) Bellare, A.; Cohen, R. E.; Argon, A. S. *Polymer* **1993**, *34*, 1393.
(24) Lee, B. J.; Argon, A. S.; Parks, D. M.; Ahzi, S.; Bartczak, Z. *Polymer* **1993**, *34*, 3555.
(25) Ajji, A.; Guevremont, J.; Cole, K. C.; Dumulin, M. M. *Polymer* **1996**, *37*, 3707.
(26) Men, Y. F.; Rieger, J.; Strobl, G. *Phys. Rev. Lett.* **2003**, *91*, 095502.
(27) Hiss, R.; Hobeika, S.; Lynn, C.; Strobl, G. *Macromolecules* **1999**, *32*, 4390.
(28) Hobeika, S.; Men, Y.; Strobl, G. *Macromolecules* **2000**, *33*, 1827.
(29) Men, Y. F.; Strobl, G. *J. Macromol. Sci., Phys B* **2001**, *40*, 775.
(30) Men, Y. F.; Strobl, G. *Macromolecules* **2003**, *36*, 1889.
(31) Galeski, A.; Argon, A. S.; Cohen, R. E. *Macromolecules* **1988**, *21*, 2761.
(32) Gupte, K. M.; Motz, H.; Schultz, J. M. *J. Polym. Sci., Part B: Polym. Phys.* **1983**, *21*, 1927.

MA051928K